Cyclooxygenase-2–dependent lymphangiogenesis promotes nodal metastasis of postpartum breast cancer

Traci R. Lyons,[1,2] Virginia F. Borges,[1,2,3] Courtney B. Betts,[1,2] Qiuchen Guo,[1,2] Puja Kapoor,[1] Holly A. Martinson,[1,2] Sonali Jindal,[1,2] and Pepper Schedin[1,2,3]

[1]Department of Medicine, Division of Medical Oncology, and [2]Young Women's Breast Cancer Translational Program, University of Colorado Anschutz, Aurora, Colorado, USA.

[3]University of Colorado Cancer Center, Aurora, Colorado, USA.

Breast involution following pregnancy has been implicated in the high rates of metastasis observed in postpartum breast cancers; however, it is not clear how this remodeling process promotes metastasis. Here, we demonstrate that human postpartum breast cancers have increased peritumor lymphatic vessel density that correlates with increased frequency of lymph node metastases. Moreover, lymphatic vessel density was increased in normal postpartum breast tissue compared with tissue from nulliparous women. In rodents, mammary lymphangiogenesis was upregulated during weaning-induced mammary gland involution. Furthermore, breast cancer cells exposed to the involuting mammary microenvironment acquired prolymphangiogenic properties that contributed to peritumor lymphatic expansion, tumor size, invasion, and distant metastases. Finally, in rodent models of postpartum breast cancer, cyclooxygenase-2 (COX-2) inhibition during the involution window decreased normal mammary gland lymphangiogenesis, mammary tumor-associated lymphangiogenesis, tumor cell invasion into lymphatics, and metastasis. Our data indicate that physiologic COX-2–dependent lymphangiogenesis occurs in the postpartum mammary gland and suggest that tumors within this mammary microenvironment acquire enhanced prolymphangiogenic activity. Further, our results suggest that the prolymphangiogenic microenvironment of the postpartum mammary gland has potential as a target to inhibit metastasis and suggest that further study of the therapeutic efficacy of COX-2 inhibitors in postpartum breast cancer is warranted.

Introduction

Postpartum breast involution, which remodels the lactation-competent breast to a nonsecretory state, occurs with weaning or after birth in the absence of lactation. In rodents and women, the process of postpartum involution is characterized by apoptosis of the mammary epithelium as well as attributes of wound healing, including increased macrophage density and fibrillar collagen deposition (1–5). These same stromal attributes also associate with tumor progression (1, 4, 6). In murine breast cancer models, postpartum mammary gland involution promotes mammary tumor growth, invasion, and metastasis (1, 3, 7). Consistent with these preclinical data, women diagnosed after childbirth and up to 5 years postpartum, cases we and others define as postpartum breast cancer (2), have increased risk for metastasis compared with age-matched nulliparous patients with similar stage disease (8–10). However the mechanism of increased metastasis in postpartum patients remains unknown. Clinically, lymph node involvement, high peritumor lymphatic vessel density, and lymphatic vessel invasion all predict metastasis in patients with breast cancer (11–16). Furthermore, lymphangiogenic growth factors VEGF-C and VEGF-D are expressed by breast tumors that display increased peritumor lymphatic vessel density, collecting lymphatic vessel dilation, and metastasis, suggesting that tumor cell–mediated induction of lymphangiogenesis can drive metastasis (15, 17–25). In adults, lymphangiogenesis has been characterized at sites of chronic inflammation, infection, wound healing, and cancer. In contrast, little is known about physiologic regulation of lymphangiogenesis in the adult mammary gland, and lymphangiogenesis has not been studied in the context of postpartum mammary gland involution (26–28). Given the reported similarities between wound healing and postpartum mammary involution (1, 3, 4, 6), we investigated the roles of lymphangiogenesis in normal mammary gland involution and in postpartum breast cancer.

In this report, we show that lymph node metastases are increased in postpartum, young-onset breast cancer cases compared with nulliparous cases, an increase that correlates with the increase in lymphatic density in the tumor microenvironment. We also show that lymphatic vessel density is increased in normal human postpartum breast tissue as well as in mammary tissue in rodent models of weaning-induced mammary gland involution. Furthermore, in rodent models of postpartum breast cancer, postpartum mice have increased peritumor lymphatic vessel density, tumor cell invasion of lymphatics, and lymph node and lung metastases compared with nulliparous mice. Importantly, postpartum tumor cells exhibit increased prolymphatic activity. Finally, we provide preclinical data implicating cyclooxygenase-2

▶ Related Commentary: p. 3704

Conflict of interest: The authors have declared that no conflict of interest exists.
Submitted: October 17, 2013; **Accepted:** June 19, 2014.
Reference information: *J Clin Invest*. 2014;124(9):3901–3912. doi:10.1172/JCI73777.

(COX-2) activity as prolymphatic in the normal involuting mammary gland and as a mediator of lymphatic metastasis of postpartum tumors. Cumulatively, our data support a role for physiologic, weaning-induced mammary gland lymphangiogenesis in the poor prognosis of postpartum breast cancer and suggest that targeting the postpartum involution window with antilymphangiogenic therapies represents a novel research avenue for this high-risk subset of breast cancer.

Results

Lymphangiogenesis in postpartum breast cancer and postpartum breast involution. To determine whether lymph node metastasis are increased in women with postpartum breast cancer, we examined the frequency of lymph node involvement at time of diagnosis in our University of Colorado young women's breast cancer cohort, which is composed of women (≤45 years of age) with breast cancer. This cohort was then refined by reproductive status into nulliparous cases and those diagnosed within 2 years postpartum. We observed a significant increase in lymph node positivity in the postpartum patients ($n = 38$) (relative risk [RR]: 1.44, 95% CI: 1.09–1.89, $P = 0.03$) compared with age-matched nulliparous patients ($n = 190$) (Figure 1A). Increased lymph node positivity is often associated with increased tumor size and/or more aggressive tumor subtypes, such as triple negative and Her2. We observed that larger tumor size increased the odds of having a positive lymph node overall in our cohort ($P < 0.0001$). However, between the nulliparous and postpartum groups, the average tumor size was not statistically different (Supplemental Figure 1A; supplemental material available online with this article; doi:10.1172/JCI73777DS1). Also, there was no observed increase in the frequency of triple-negative or Her2-positive cases in the postpartum group (Figure 1B). These data suggest that a recent pregnancy, in this case being within 2 years of childbirth, may influence the frequency of lymph node metastasis. To examine whether peritumoral lymphatic vessel density is also increased in these postpartum breast cancers, we compiled a young women's stage II breast cancer tissue set balanced for tumor estrogen receptor (ER), progesterone receptor (PR), and Her2 receptor status and grouped by time since last birth at diagnosis (Supplemental Figure 1B). We stained these specimens for podoplanin (D2-40), the clinically utilized marker of lymphatic endothelium (29), and calculated the number of podoplanin$^+$ lymphatics per area in the peritumor region. Breast tumors diagnosed ≤3 years postpartum had a significant increase in lymphatic vessel density compared with breast tumors diagnosed in nulliparous women or those diagnosed >3 years postpartum (Figure 1C). Importantly, ER, PR, and/or Her2 status of the tumors did not significantly influence the number of peritumoral podoplanin$^+$ vessels, highlighting the potential role of a postpartum diagnosis on tumor-associated lymphangiogenesis (Figure 1D). In addition, a significant correlation between peritumoral lymphatic vessel density and tumor cell invasion of lymphatics was observed (Figure 1E), and many of the histologically identified tumor cells observed in lymphatic vessels stained positive for Ki67 (Figure 1F), demonstrating viability. Cumulatively, these data suggest that the increased tumor-associated lymphangiogenesis observed in postpartum breast cancers may contribute to the overall poor prognosis of this patient population by facilitating increased lymph node metastases.

One potential explanation for why lymphatic density is increased in the postpartum breast cancers is because the unique microenvironment of the postpartum gland specifically supports lymphangiogenesis. Thus, we investigated whether breast tissue lymphatic vessel density is increased during postpartum involution. Lymphatic vessel density was significantly elevated in the normal adjacent breast tissue obtained from women ≤1-year postpartum compared with that in all other groups, suggesting that expansion of the lymphatic vasculature occurs in the postpartum breast (Figure 1G). Further, lymphatic vessels in human breast tissues collected 4 to 6 weeks after weaning contained cellular debris, indicating a possible role for lymphatics in the clearance of apoptotic alveolar cells during postpartum gland involution (Figure 1H). A potential caveat of our lymphatic vessel density analysis is that these histologically normal breast tissue sections were obtained from patients with breast cancer and, thus, signals from the tumor cells may contribute to the observed increased lymphatic vessel density. However, in the ≤1-year postpartum breast tissues there was no significant reduction in lymphatic vessel density in lobules obtained from distinct quadrants of the breast and from the contralateral breast that lacked tumor cells. Furthermore, we did not observe any correlation between proximity to tumor and lymphatic vessel density (Supplemental Figure 1, C and D). Finally, since our cohorts are balanced for breast cancer stage and subtype, the observation that adjacent normal lymphatic vessel density is elevated specifically in the cases diagnosed ≤1-year postpartum is consistent with the reproductive state of the host being the determinant of lymphatic density, rather than the presence of cancer.

Physiologic mammary lymphangiogenesis in postpartum rodent models. We next investigated lymphangiogenesis during weaning-induced involution under the highly synchronized conditions that rodent models permit. We quantitated LYVE1, a marker of initial lymphatics (30), in rat and mouse mammary tissues across the reproductive stages of pregnancy, lactation, and weaning-induced involution. Increased LYVE1$^+$ mammary lymphatic vessel density was observed at 3 to 4 days after lactation/weaning (InvD3–4) in comparison with that at nulliparous, pregnant, and lactation time points, with vessel density peaking at mid to late involution (InvD6–10) in 4 independent models: SD rats (Figure 2A), BALB/c mice (Figure 2B), and C57/BL6 and SCID mice (Supplemental Figure 2, A and B). Rat mammary *Lyve1* mRNA expression was also increased during involution (Figure 2C). We next focused on gene expression of known prolymphangiogenic molecules during the pregnancy-lactation-involution cycle in rat mammary tissues and observed increased gene expression of *Vegfc* and *Vegfd* and their receptors *Vegfr2* and *Vegfr3* at involution day 8, just prior to the peak in LYVE1$^+$ vasculature, demonstrating that gene programs associated with lymphangiogenesis are activated in the postpartum mammary gland (Figure 2, D–G). To examine early stages of lymphatic vessel expansion during mammary gland involution, we evaluated changes in lymphatic vessel density between 2 and 4 days after weaning (InvD2–4). In both rat and SCID mice, the observed increase in mammary lymphatic density was preceded, at InvD2, by a transient increase in single LYVE1$^+$ cells and/or small LYVE1$^+$ vessels (Figure 2, H and I, and Supplemental Figure 2B), suggesting that an influx or expansion of LYVE1$^+$ cells contributes to the lymphatic vessel formation observed during involution.

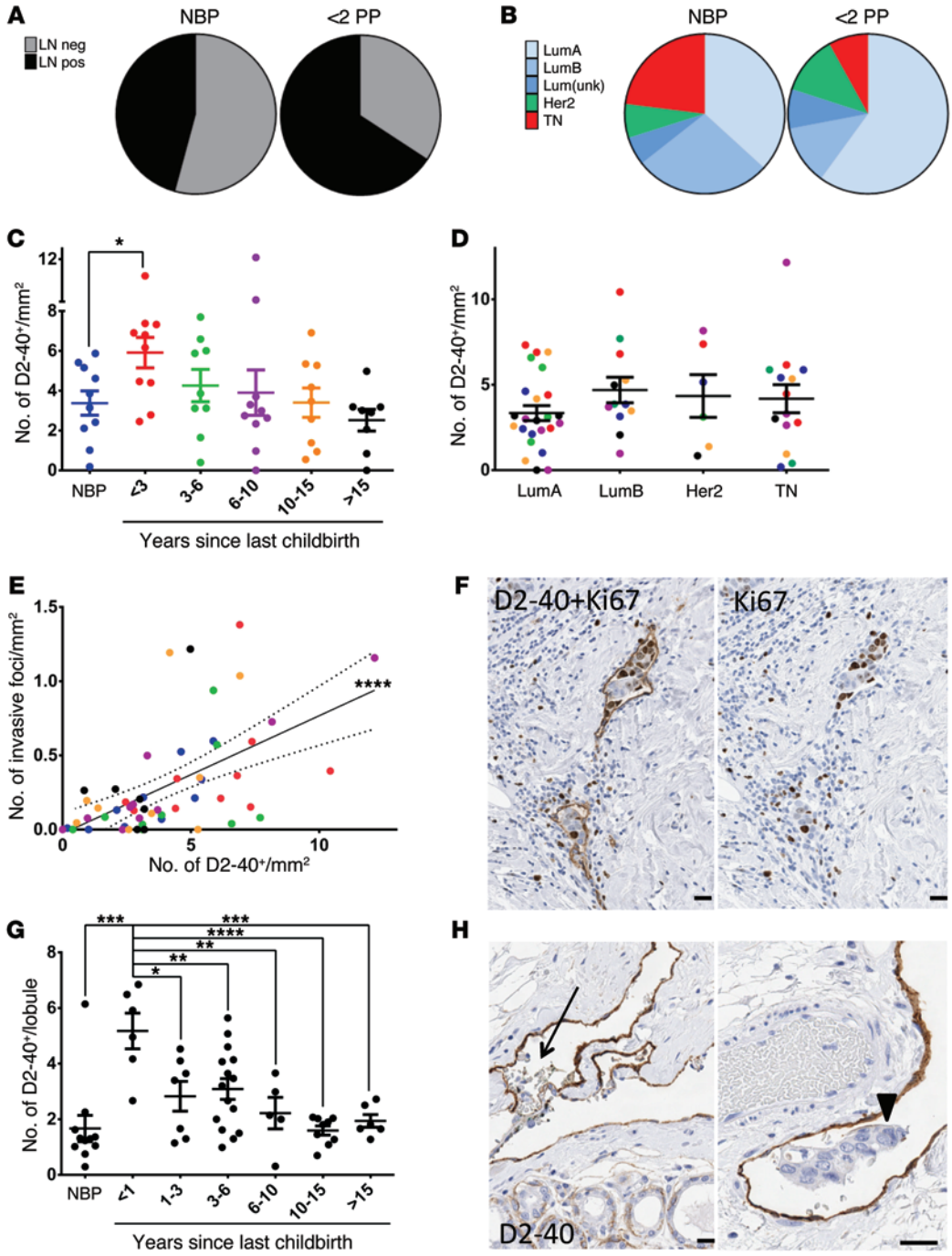

Figure 1. Postpartum breast cancers exhibit increased lymph node metastasis and lymphatic vessel density. (**A**) Percentage of lymph node (LN) positivity is increased in women diagnosed with breast cancer within 2 years postpartum (<2 PP) (n = 38) compared with women who have never been pregnant (NBP) (n = 190). (**B**) Similar percentages of tumor subtypes are observed in postpartum and nulliparous groups: luminal A (LumA), luminal B (LumB), unknown luminal [Lum(unk)] (ER status was positive but PR unknown), Her2, or triple-negative (TN) subtype. (**C**) Peritumor D2-40$^+$ vessel density is increased in breast cancers diagnosed within 3 years of last childbirth (<3) in comparison to that in women who have never been pregnant (exact P = 0.0186). (**D**) Increased peritumor D2-40$^+$ vessel density observed in the <3 group is not significantly increased by any known tumor biologic subtype. Color coding shows the reproductive-based tumor categories when separated by subtype. (**E**) D2-40$^+$ vessel density correlates with number of D2-40$^+$ vessels containing tumor cell nuclei (Pearson r = 0.5811). (**F**) Representative image of tumor cell lymphatic invasion in a D2-40$^+$/Ki67-stained breast cancer specimen. Tissue sections were stained for Ki67 (right) then for D2-40 (left). (**G**) D2-40$^+$ lymphatic vessel density is increased in normal adjacent breast tissue from women biopsied less than or equal to 1-year postpartum (≤1), compared with women biopsied 1–3 (>1≤3), 3–6 (>3≤6), 6–10 (>6≤10), 10–15 (>10≤15), and greater than 15 (>15) years postpartum and women who have never been pregnant. (**H**) Representative image depicting D2-40$^+$ vessels containing cellular debris (arrow) or cells (arrowhead) in breast tissue obtained during 2 weeks after lactation. All data points are depicted along with group average (black bar ± SEM). Scale bar: 10 μm. *P < 0.05, **P < 0.01, ***P < 0.001, ****P < 0.0001, t test.

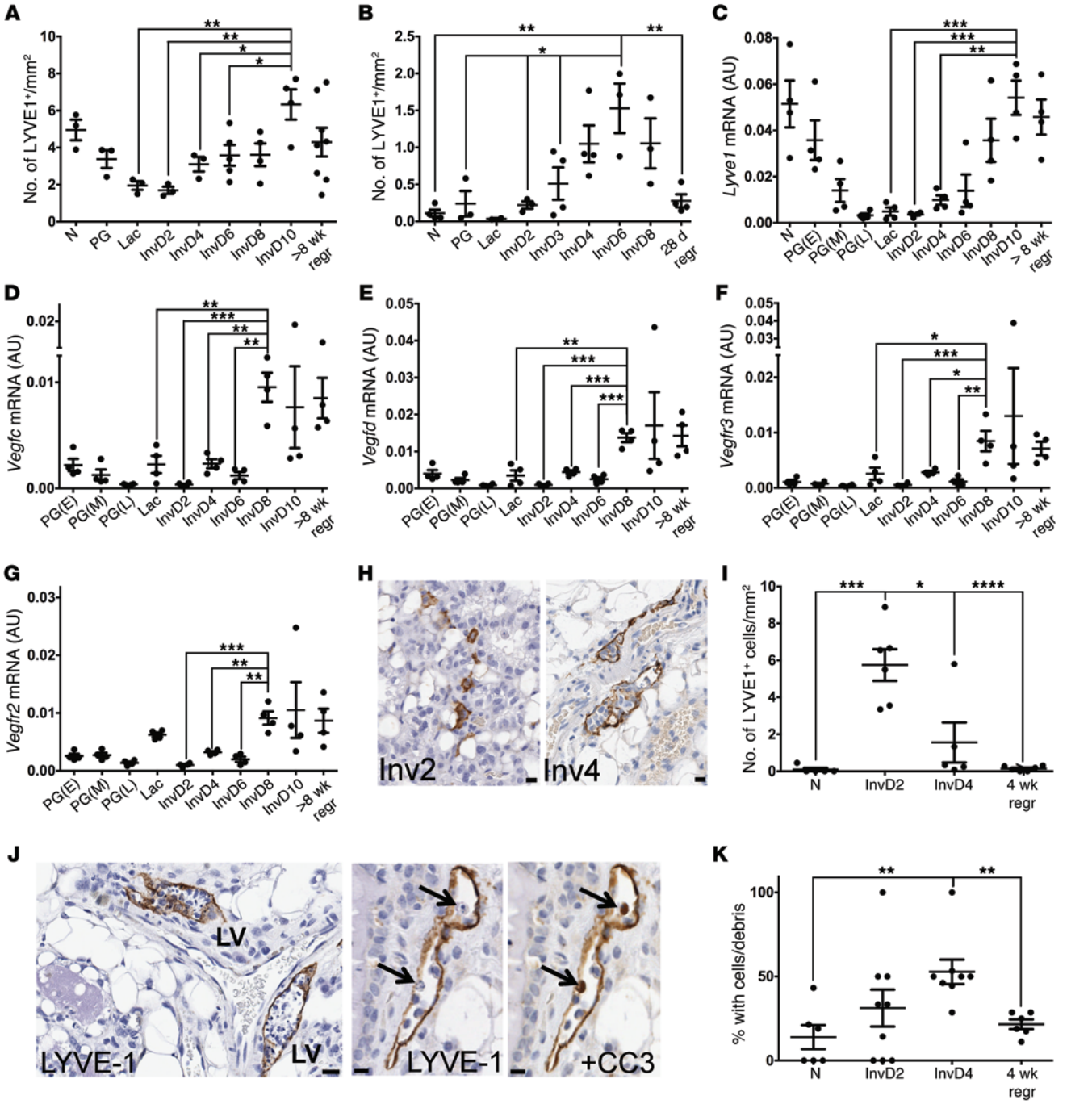

Figure 2. Involution-specific lymphangiogenesis is COX-2 dependent. (**A**) Mammary LYVE1$^+$ vessel density increases during postpartum involution in the rat. N, nulliparous; PG, pregnant; Lac, lactating; >8 wk regr, 8-week regressed. (**B**) Increased LYVE1$^+$ vessel density during involution in BALB/C mouse mammary tissue. Increased mRNA expression during involution (normalized to actin) of (**C**) *Lyve1*, (**D**) *Vegfc*, (**E**) *Vegfd*, (**F**) *Vegfr3*, and (**G**) *Vegfr2*. (**H**) Representative images of LYVE1-stained SCID mouse mammary tissue. (**I**) Increased LYVE1$^+$ single cells per mm^2 in SCID mouse mammary tissue at InvD2. (**J**) Representative image of cell debris in LYVE1$^+$ vessels (LV). Arrows depict condensed nuclei that are also CC3$^+$. Tissues were initially stained for LYVE1 to identify lymphatics (center), followed by CC3 on the same tissue section to identify apoptotic cells (right). (**K**) LYVE1$^+$ vessels with cell debris increase during involution. All data points are depicted along with group average (black bar ± SEM). Scale bar: 10 μm. $^*P < 0.05$, $^{**}P < 0.01$, $^{***}P < 0.001$, $^{****}P < 0.0001$, *t* test.

Furthermore, consistent with a role for lymphatic vasculature in the clearance of apoptotic cells during involution, murine tissues from day 4 of involution dual stained for LYVE1 and cleaved caspase-3 (CC3) revealed an increase in mammary lymphatic vessels containing CC3$^+$ apoptotic cells and other cellular material (Figure 2, J and K). We also confirmed the presence of cells and cellular debris in lymphatics at day 4 of involution in rat mammary tissues (Supplemental Figure 2D). These results demonstrate that expansion of the lymphatic vasculature occurs during postpartum mammary gland involution in rodents and are consistent with the

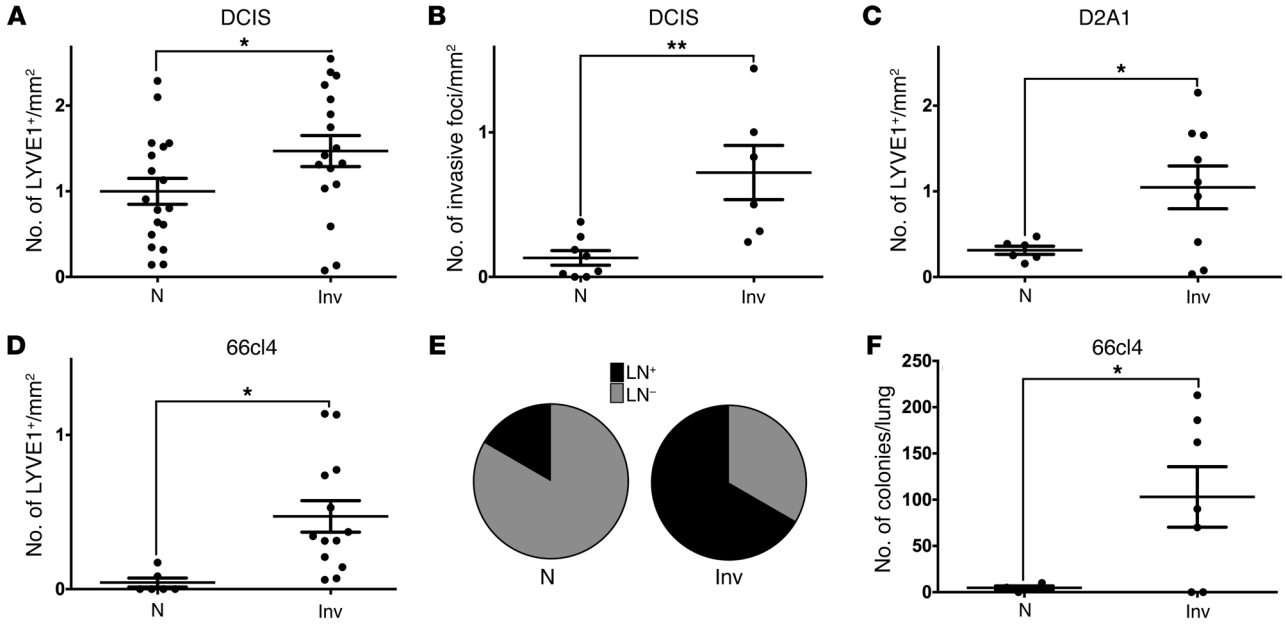

Figure 3. Mouse models of postpartum breast cancer have increased peritumoral lymphatic vessel density, tumor cell lymphatic vessel invasion, and lymph node and lung metastases. (**A**) Increased peritumoral LYVE1$^+$ vessel density and (**B**) number of LYVE1$^+$ vessels containing MCF10DCIS tumor cell nuclei in involution (Inv) compared with nulliparous hosts. (**C** and **D**) Increased peritumoral LYVE1$^+$ vessel density with orthotopic injection of murine (**C**) D2A1 or (**D**) 66cl4 cells into involution compared with nulliparous hosts. (**E**) Percentage mice with (+) axillary lymph nodes is increased in involution group animals compared with nulliparous controls (n = 18 per group). (**F**) Number of colonies per lung is increased in size-matched tumors in the involution compared with nulliparous group. All data points are depicted along with group average (black bar ± SEM). $^*P < 0.05$, $^{**}P < 0.01$, t test.

increased lymphatic vessel density observed in the adjacent normal tissue of postpartum women described above.

Mammary involution affects lymph node metastasis in postpartum tumor models. We next addressed whether tumor cell exposure to the prolymphatic environment of the normal involuting mammary gland results in increased peritumor lymphatic vessel density and tumor cell lymphatic invasion in rodent models of postpartum breast cancer. Human MCF10DCIS cells were injected into mammary fat pads of age-matched nulliparous or postpartum SCID mice at day 1 of involution, and tumors were harvested 8 weeks after injection. Tumors from the postpartum group had increased peritumoral lymphatic vessel density and tumor cell invasion into lymphatic vessels compared with that in the nulliparous control group, even after controlling for tumor size (Figure 3, A and B, and Supplemental Figure 3, A and B). We also confirmed increased peritumoral lymphatic vessel density in the postpartum group in 2 additional immune-competent models, using the D2A1 and 66cl4 murine mammary tumor cell lines (Figure 3, C and D). To ascertain whether expanded lymphatic vasculature associated with metastatic seeding, we examined lymph node and lung metastasis in the 66cl4 cell murine model, as this cell line preferentially disseminates via the lymphatics (31). We observed increased tumor size in the postpartum hosts (Supplemental Figure 3C) as well as increased axillary lymph node positivity (Figure 3E) (RR: 2.5, CI: 1.2–5, P = 0.006) and increased lung metastasis (Figure 3F), even after controlling for tumor size (Supplemental Figure 3D). In addition to increased incidence of metastasis, the number and size of lung micrometastases were higher in the postpartum group (Supplemental Figure 3, E and F).

Our observation that mammary gland lymphangiogenesis is activated during postpartum involution, combined with the observation that lymphatic vessel density is elevated in postpartum tumors after gland involution is complete, indicates that tumor cells present during involution may acquire prolymphangiogenic attributes that persist after the completion of normal mammary gland involution. To address this question, we isolated involution or nulliparous group tumor cell populations from our DCIS.COM xenograft model and assessed for the ability of these tumor cells to influence lymphatic endothelial cell (LEC) migration ex vivo, an important early step during lymphangiogenesis in vivo (32). In transwell filter assays, significantly more LECs migrated toward postpartum tumor cells (Supplemental Figure 4A) and their conditioned media (Figure 4A) than toward nulliparous tumor controls. To determine whether postpartum tumor cells can promote lymphatic structure formation, we performed LEC tube formation assays in the presence of tumor cell–conditioned media. Quantitation of the surface area occupied by the lymphatic structures per well and the number of branches per well revealed that postpartum tumor cell–conditioned media resulted in LEC structures that were larger (Figure 4B) and more branched (Figure 4C). Furthermore, we observed increased lymphatic expression of junctional VE-cadherin protein in LEC structures exposed to postpartum tumor cell–conditioned media (Figure 4, D and E) compared with that in those exposed to nulliparous control media (Supplemental Figure 4, B and C). While postpartum tumor cell–conditioned media did not promote proliferation of LECs (Supplemental Figure 4D), evidence of decreased expression of CC3 by immunoblot revealed a potential role in suppression of LEC death (Figure 4F). To examine

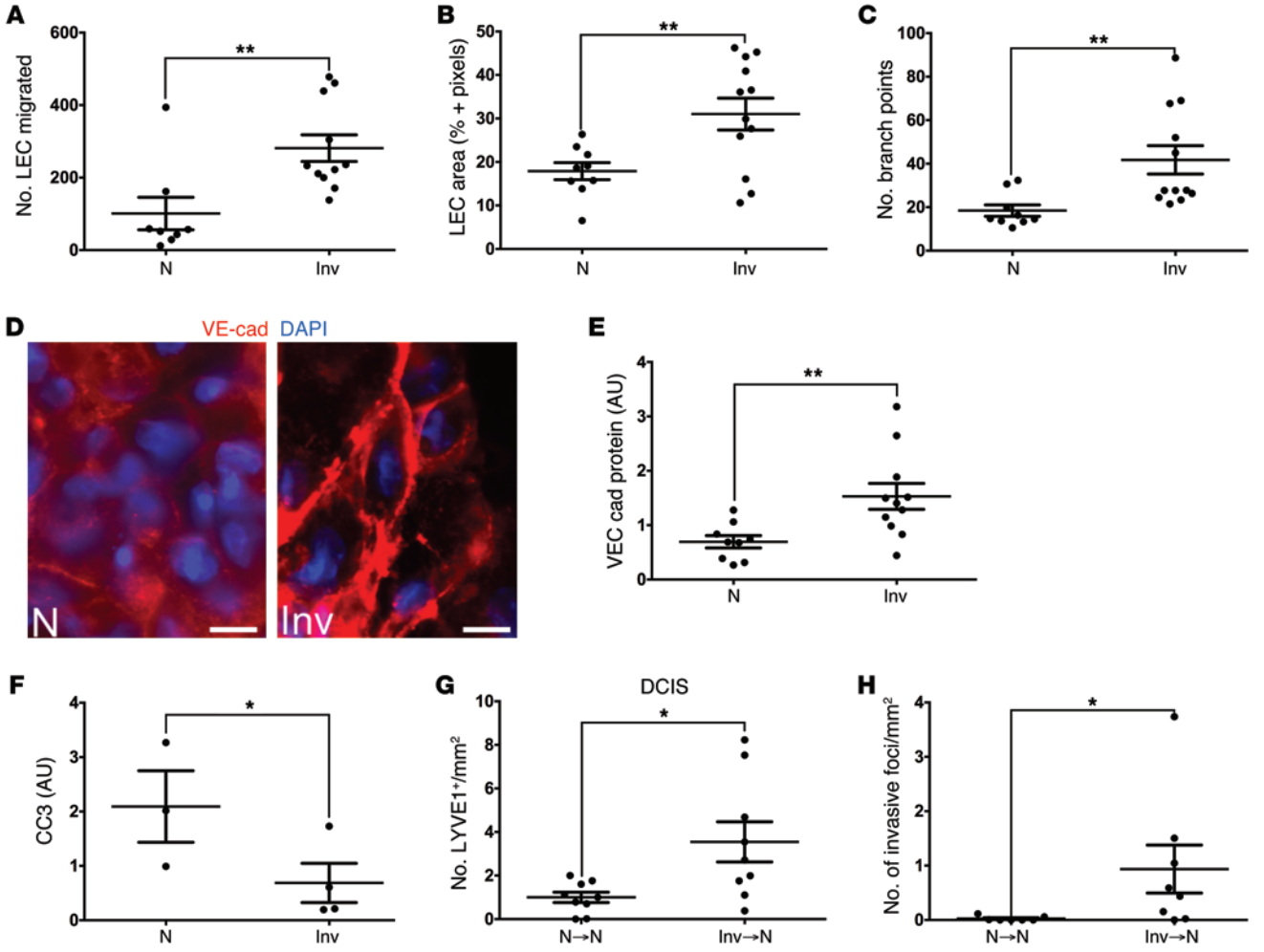

Figure 4. Postpartum tumor cells promote lymphangiogenesis and express increased VEGF-C. Conditioned media from tumor cell populations collected from postpartum mice injected with MCF10DCIS tumor cells at day 1 of involution ($n = 4$) increased (**A**) LEC migration and LEC organoid complexity, as measured by (**B**) surface area, (**C**) organoid branching, and (**D** and **E**) VE-cadherin protein expression in tube formation assays, in comparison to nulliparous tumor cell (N, $n = 3$) conditioned media. Data from 2 to 3 replicate experiments per cell line are shown. Representative IF images of LEC organoids showing increased junctional VE-cadherin with conditioned media from involution group tumor cells compared with nulliparous media. (**F**) CC3 protein expression is decreased in LEC organoids cultured in conditioned media from involution group tumor cells. Involution group tumor cell populations also increase (**G**) peritumor LYVE1$^+$ vessel density and (**H**) number of LYVE1$^+$ vessels containing tumor cell nuclei when injected into nulliparous hosts (Inv→N) compared with nulliparous group tumor cells (N→N). All data points are depicted along with group average (black bar ± SEM). Scale bar: 5 μm. $^*P < 0.05$, $^{**}P < 0.01$, *t* test.

whether postpartum tumor cells could promote lymphangiogenesis in vivo, we injected freshly isolated postpartum and nulliparous tumor cells into mammary fat pads of nulliparous hosts and observed significantly elevated peritumor lymphatic vessel density and lymphatic invasion in the group injected with postpartum tumor cells (Figure 4, G and H). Together, these results indicate that tumor cell exposure to the involution mammary microenvironment results in a gain of prolymphangiogenic attributes that are maintained even after removal from postpartum hosts. Further, these results suggest that a postpartum event could drive phenotypic changes in human breast cancers diagnosed at time points after breast involution has occurred.

COX-2 promotes postpartum lymphangiogenesis. We have shown that DCIS.COM tumor cells from the postpartum group (postpartum tumor cells) overexpress COX-2 compared with DCIS.COM cells derived from nulliparous group tumors (1), and here, we provide independent validation of this data (Supplemental Figure 4F). To begin to evaluate for potential interactions between COX-2 and the promotion of lymphangiogenesis, we examined the lymphangiogenic-inducing properties of DCIS.COM cells with COX-2 knocked down (shCOX-2 MCF10DCIS cells, referred to herein as shCOX-2 cells). First, conditioned media isolated from shCOX-2 cells resulted in an approximately 38% decrease in LEC structure branching in vitro compared with vector controls (shGFP MCF10DCIS) (Figure 5A). Furthermore, injection of shCOX-2 cells into postpartum hosts resulted in a 60% decrease in peritumor lymphatic vessel density and an 85% decrease in tumor cell invasion of lymphatics, compared with size-matched vector control tumors (Figure 5, B and C, and Supplemental Figure 5A). Because we also observed decreased overall tumor size and COX-2 expression in the shCOX-2 group compared with controls (Supplemental Figure 5B), we examined the correlation between lymphatic vessel

density and tumor size and/or COX-2 expression. While we did not observe a correlation between lymphatic vessel density and tumor size (Supplemental Figure 5C), we did observe a positive correlation ($r = 0.6354$) between COX-2 expression and lymphatic vessel density (Figure 5D), data that further implicates a role for tumor cell COX-2 expression in promoting peritumoral lymphangiogenesis.

COX-2 catalyzes the conversion of arachidonic acid to prostaglandin endoperoxide H2 that serves as the precursor to prostaglandins (PGD2, PGE_2, PGF2α) (33, 34). To determine whether COX-2 activity in postpartum tumor cells promotes lymphangiogenesis via increased production of prostaglandins, we measured PGE_2, as PGE_2 has been reported to promote lymphangiogenesis (35). We observed increased PGE_2 in postpartum tumor cells and conditioned media compared with that in nulliparous controls, as measured by ELISA (Figure 5, E and F). Furthermore, human dermal LECs cultured in the presence of postpartum tumor cell–conditioned media had increased expression of the EP2 receptor, a receptor for PGE_2, as assessed by immunoblotting (Figure 5G), suggesting that PGE_2 production by postpartum tumor cells influences lymphangiogenesis via increased EP2 receptor on the LECs. Consistent with this hypothesis, when exogenous PGE_2 was added to nulliparous media, LEC surface area was increased to levels more similar to those observed with postpartum media (Figure 5H). Importantly, addition of an EP receptor antagonist AH6809, which has been shown to have high affinity for the EP2 receptor, into postpartum media suppressed LEC surface area to levels similar to those observed in nulliparous controls (Figure 5H). Branching was also reduced with the EP receptor antagonist (Figure 5I), indicating that involution group tumor cells promote survival and branching of lymphatic structures via EP receptor(s) signaling.

To evaluate the role of COX-2 activity in expansion of the lymphatic vasculature during normal postpartum mammary gland involution in vivo, postpartum mice were fed celecoxib (CXB) during involution as described previously (1). CXB is a highly selective inhibitor of COX-2 that inhibits the transformation of arachidonic acid to prostaglandin precursors (36). In normal mammary tissues harvested at day 4 of involution, we observed a significant decrease in mammary lymphatic vessel density in postpartum animals treated with CXB, with no observable effects on overall mammary gland morphology or the normal secretory epithelial cell apoptosis that occurs during involution (Figure 5J and Supplemental Figure 5, D and E). These results suggest that COX-2 activity promotes physiologic lymphangiogenesis during normal involution. To investigate whether COX-2 inhibition during involution was also sufficient to decrease postpartum tumor-associated lymphangiogenesis, lymphatic vessel invasion, and lung metastases, CXB treatment was administered for 14 days after weaning in our xenograft tumor model, and tumors harvested 4 to 6 weeks after CXB treatment. Tumors from the CXB-treated involution group exhibited 48% and 60% reductions in lymphatic vessel density and lymphatic invasion, respectively, compared with the untreated involution group tumors (Figure 5, K and L). Furthermore, lung micrometastases were reduced by 80% in the CXB-treated involution group (Figure 5M and Supplemental Figure 5F). Importantly, we also confirmed these results in the immunecompetent 66cl4 tumor model, in which we observed decreased lymphatic vessel density and lung metastasis with CXB treatment (Figure 5, N and O). Collectively, these results suggest that COX-2 activity mediates lymphangiogenesis in the normal postpartum gland and promotes the prolymphangiogenic and metastatic properties observed in postpartum tumor cells. Further, our results indicate that inhibition of COX-2 during involution is sufficient to decrease postpartum tumor-associated lymphangiogenesis, lymphatic vessel invasion, and lung metastasis, without interfering with normal weaning-induced gland regression.

Discussion

We have previously identified the period of murine postpartum mammary gland involution as a window of risk for metastatic spread of human breast cancer cells; however, the mechanism of tumor cell escape from the mammary gland was not identified (1). Current analysis of our young women's breast cancer cohort reveals that lymph node metastases were significantly increased in patients with breast cancer diagnosed within 2 years postpartum. Further, this increased metastasis appears to be independent of tumor size and clinically defined breast cancer subtypes designated by ER, PR, and/or Her2 status. We also found that the lymphatic vasculature is expanded in the normal breast tissue of early postpartum women, suggesting a physiologic role for lymphatics in the clearance of apoptotic secretory epithelial cells during the postpartum involution process. Further, we observed an increase in tumor-associated lymphatics in a cohort of postpartum breast cancers, which correlates with increased lymphatic vessel invasion. These results suggest that physiologically normal lymphangiogenesis that occurs in the postpartum involuting breast may facilitate breast cancer dissemination in postpartum women, an observation that may explain the increased lymph node metastasis in our postpartum patient population as well as the published increased risk for metastatic disease observed in this patient population (8–10).

We have modeled the interaction between postpartum involution and lymphatic mediated metastasis using multiple rodent models. While angiogenesis has been characterized in rodent mammary glands during pregnancy, lactation, and involution (37–39), the observation that lymphatic vessel density increases during the normal developmental process of mammary gland involution is novel. Furthermore, the observation that lymphatic vessel density is increased in the microenvironment of postpartum tumors in women and in our mouse models of postpartum breast cancer suggests that increased mammary lymphatic vessel density during involution is a dominant feature across species that may facilitate breast cancer lymphogenous spread. We also show that tumor cells exposed to the involuting mammary gland microenvironment acquire prolymphangiogenic attributes, including upregulation of COX-2 and PGE_2, a product of COX-2 activity, which persist after exposure to this transient event. Thus, a positive feedback loop between physiologic lymphangiogenesis and tumor cell–mediated lymphangiogenesis that involves upregulation of COX-2 activity may be established in postpartum breast tumors. In addition, we show that human tumor cells with stable knockdown of COX-2 exhibit decreased postpartum tumor-associated lymphatic vessel density, suggesting that COX-2 may be necessary for tumor cells to respond to the prolymphangiogenic signals during involution. Finally, we have shown recently that

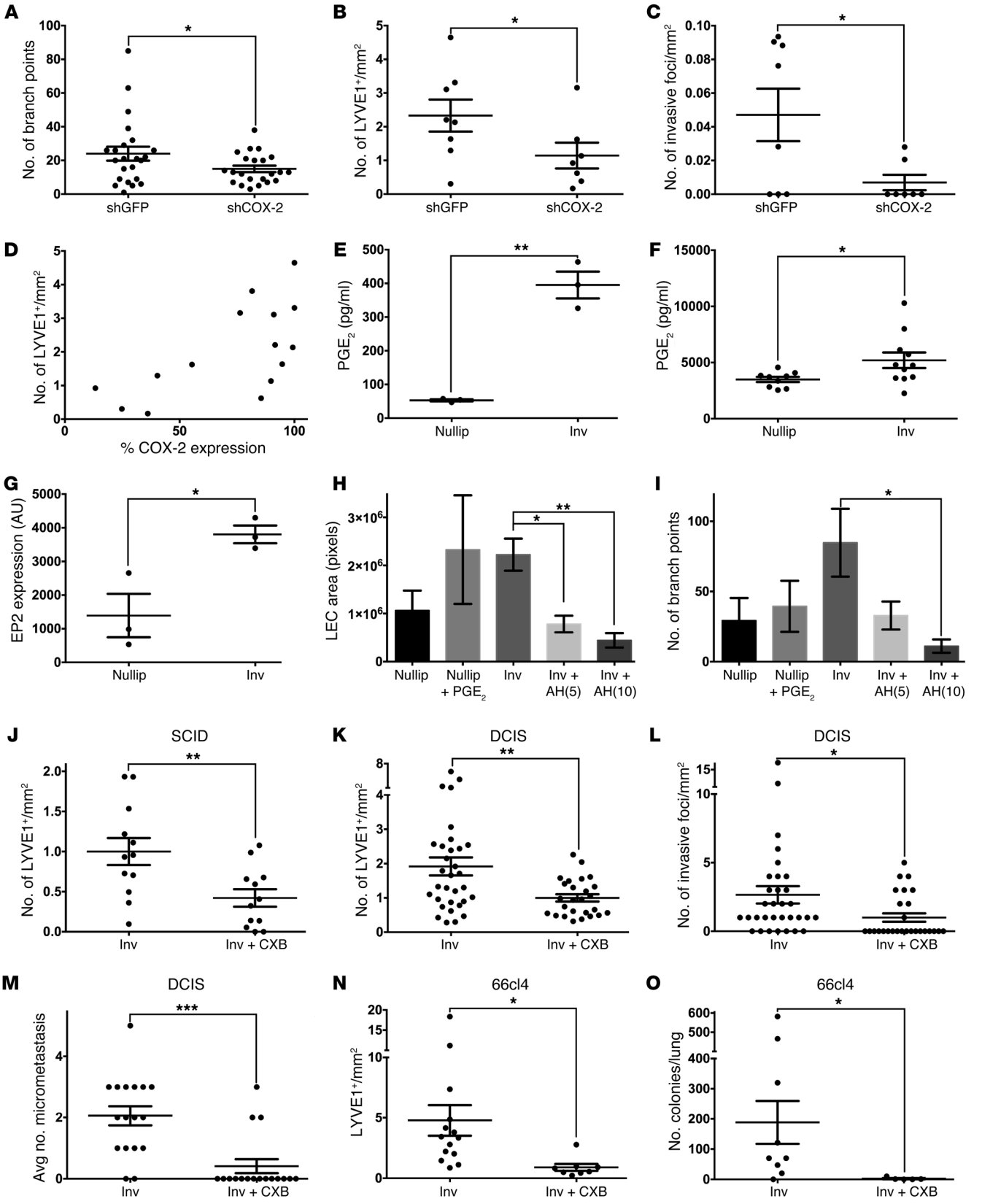
A
No. of branch points
shGFP
shCOX-2
B
No. of LYVE1+/mm2
shGFP
shCOX-2
C
No. of invasive foci/mm2
shGFP
shCOX-2
D
No. of LYVE1+/mm2
% COX-2 expression
E
PGE2 (pg/ml)
Nullip
Inv
F
PGE2 (pg/ml)
Nullip
Inv
G
EP2 expression (AU)
Nullip
Inv
H
LEC area (pixels)
Nullip
Nullip + PGE2
Inv
Inv + AH(5)
Inv + AH(10)
I
No. of branch points
Nullip
Nullip + PGE2
Inv
Inv + AH(5)
Inv + AH(10)
J
SCID
No. of LYVE1+/mm2
Inv
Inv + CXB
K
DCIS
No. of LYVE1+/mm2
Inv
Inv + CXB
L
DCIS
No. of invasive foci/mm2
Inv
Inv + CXB
M
DCIS
Avg no. micrometastasis
Inv
Inv + CXB
N
66cl4
LYVE1+/mm2
Inv
Inv + CXB
O
66cl4
No. colonies/lung
Inv
Inv + CXB

Figure 5. COX-2–dependent lymphangiogenesis, lymphatic vessel invasion, and lung metastasis in a xenograft model of postpartum breast cancer. (**A**) shCOX-2 cells induce fewer branches in tube formation assays compared with shGFP MCF10DCIS (shGFP) vector controls. (**B**) Injection of shCOX-2 cells during involution results in decreased peritumoral LYVE1$^+$ vessel density and (**C**) number of LYVE1$^+$ vessels containing tumor cell nuclei compared with vector control cells. (**D**) Tumor cell COX-2 expression correlates with tumor-associated LYVE1$^+$ vessel density (Pearson $r = 0.6354$). Involution group tumor cell (**E**) lysates and (**F**) conditioned media contain higher levels of PGE_2 by ELISA. (**G**) LECs cultured in involution group tumor cell–conditioned media upregulate EP2 protein expression. (**H**) LECs cultured in nulliparous media and 10 μM PGE_2 form larger structures, and LECs cultured in involution group tumor cell–conditioned media and EP2 antagonist (AH6809) at 5 μM and 10 μM form smaller structures (**I**) with fewer branches. In involution group animals, CXB diet (Inv+CXB) decreases (**J**) LYVE1$^+$ vessel density in SCID mouse mammary glands during normal involution, (**K**) peritumoral LYVE1$^+$ vessel density, (**L**) number of LYVE1$^+$ vessels containing tumor cell nuclei, and (**M**) average number of lung micrometastasis per animal. CXB diet also decreased (**N**) peritumoral LYVE1$^+$ vessel density and (**O**) lung metastasis in BALB/c mice with 66cl4 mammary tumors. All data points are depicted along with group average (black bar ± SEM). $^*P < 0.05$, $^{**}P < 0.01$, $^{***}P < 0.001$, *t* test.

COX-2 is upregulated in mammary epithelial cells during involution (40), and here, we show that prolymphangiogenic growth factors VEGF-C and VEGF-D were similarly upregulated. Given that COX-2 has been shown to regulate both VEGF-C and VEGF-D (18, 41), the possibility that COX-2 also promotes lymphangiogenesis in the breast via regulation of VEGF-C and VEGF-D cannot be ruled out by the results presented herein.

Our previously published results using a xenograft model of postpartum breast cancer indicate that systemic inhibition of COX-2 activity with NSAIDs during mammary gland involution is sufficient to decrease tumor-promoting collagen, tumor cell expression of COX-2, local invasion by postpartum tumor cells, and lung metastasis (1). Here, we extend these studies by demonstrating that lymphangiogenesis is a normal physiologic process that occurs during postpartum mammary gland involution, which is similarly decreased by COX-2 inhibition. Further, COX-2 inhibition targeted to postpartum involution reduces tumor-associated lymphatic vessel density and inhibits tumor cell invasion into lymphatic vessels. Also, we show for the first time that COX-2 inhibition reduces lung metastasis in an immune-competent model. Our in vitro results suggest that COX-2 activity promotes tumor cell secretion of PGE_2 and affects expansion of tumor-associated lymphatic vasculature through the EP2 receptor. Thus, COX-2 inhibition during involution may block establishment of a feedback loop that results in increased PGE_2 production by postpartum tumor cells, thereby reducing peritumor lymphatic vessel density, lymphatic vessel invasion by tumor cells, and possibly lymphogenous spread. Whether COX-2 inhibition is also acting directly on the lymphatic vasculature is unanswered by our current studies and merits further investigation. Furthermore, macrophages are an additional cell type thought to play crucial roles in both normal and tumor-associated lymphangiogenesis (30, 42–44). Since macrophages are increased in the postpartum involuting gland (4, 45), we also recognize the importance of determining whether macrophages are driving lymphangiogenesis in the postpartum mammary gland.

In summary, our results support the idea that COX-2–dependent signals during the involution window promote tumor-associated lymphangiogenesis, which thereby suggests that COX-2–targeting interventions or combination interventions with COX-2 inhibitors and other antilymphangiogenic-based therapies are a promising research strategy for reducing lymphatic mediated metastasis in this high-risk patient population. In support of this, in trials of long-term daily aspirin use, subjects with daily aspirin use who developed any type of cancer exhibited decreased incidence of distant metastasis compared with control subjects (46). Furthermore, multiple prolymphangiogenic molecules have been proposed as candidates for safe pharmacological inhibition of lymphangiogenesis (47–50), and monoclonal antibody–based antilymphatic therapies are already in clinical trials (30, 51). Thus, postpartum-targeted antiinflammatory/antilymphangiogenesis strategies may prove to be safe and clinically beneficial for the 30% to 35% of all women with young-onset breast cancer who are likely to be within 5 years of pregnancy at diagnosis (52, 53).

Methods

Analysis of clinical cohort for lymph node involvement. Cases were identified through our young women's breast cancer database and tissue collection, which was created under a Colorado Multiple Institution Review Board–approved and subject consent–exempt protocol. The cases were sorted in RedCap based on the following chart review criteria: age, ≤45 at diagnosis; verified premenopausal; parity, nulliparous cases had never been pregnant and parous cases had at least 1 full-term pregnancy; and lymph node status, nodal AJCC stage was N0 for lymph node negative and N ≥ 1 for lymph node positive. Tumor size, ER, PR, and Her2 status data were also collected for each case used in the analysis. Cases were grouped according to common clinical subtypes as follows: luminal A ($ER^+/PR^+/Her2^-$), luminal B ($ER^+/PR^-/Her2^-$, $ER^+/PR^+/Her2^+$, or $ER^+/PR^-/Her2^+$), Her2 positive ($ER^-/PR^-/Her2^+$), or triple negative ($ER^-/PR^-/HER2^-$). For some cases, only ER positivity was known, with PR and Her2 unknown, resulting in a luminal unknown category. Tumor size was unknown in 22 nulliparous cases.

Human tissues. Deidentified human breast tissue was obtained through the same protocol as outlined above. Normal adjacent and tumor tissues were grouped according to years since last childbirth or as never been pregnant (nulliparous) for analysis of lymphatic vessel density and lymphatic vessel invasion. Never been pregnant cases were used for the nulliparous cohort in order to eliminate confounding of the data by pregnancies that did not result in live births.

Cell culture. MCF10DCIS.COM-GFP (and shRNA derivatives) were obtained from K. Polyak (Harvard University, Cambridge, Massachusetts, USA), and 66cl4-luciferase cells (54) were obtained from H. Ford (University of Colorado, Boulder, Colorado, USA). Cells were cultured as described previously (1, 31, 55). Human dermal LECs (HDLECs) were obtained from PromoCell and maintained according to manufacturer's protocol with the following modifications: for routine culturing, plates were coated with 10 μg/ml Matrigel.

Animal studies. Rodent breeding, tissue acquisition, and staining were performed as described previously (1, 4). Animal procedures were approved with ethical consideration by the University of Colorado Anschutz Medical Campus Institutional Animal Care and Use Committee. For the tumor models, 200,000 DCIS-GFP (xenograft), 20,000 D2A1 (isograft), or 200,000 66cl4-LUC (isograft) cells were

injected into right and left no. 4 mammary glands of SCID or BALB/c dams 1 day after weaning (postpartum or involution group) or into age-matched nulliparous mice. Based on primary tumor cell growth, mice were sacrificed at 8 weeks after injection (DCIS xenograft), 5 weeks after injection (D2A1), or 4 to 5 weeks after injection (66cl4). Tumor cell populations were obtained from xenograft mammary tumors 3 weeks after injection and reinjected (200,000 cells) into nulliparous SCID animals. In vivo studies were replicated twice with representative or pooled data shown. For both normal and tumor studies, CXB (Pfizer) was delivered by published methods at 500 mg/kg diet (1), starting at day 10 of lactation and ending at day 14 of involution.

Tumor cell population isolation. Excised mammary tumors were rinsed in ice-cold PBS, minced and digested with 2 mg/ml collagenase (Sigma-Aldrich) and 10 μg/ml hyaluronidase (Sigma-Aldrich) in complete media plus amphotericin B (0.25 μg/ml) (MP Biomedicals) and penicillin and streptomycin (100 units/100 μg) (Hyclone). Following shaking at 37°C for 3 hours, cells were pelleted, washed, plated in complete media, grown to confluence, and used for in vitro assays. Frozen cell pellets were also obtained for mRNA and protein analyses.

Immunohistochemistry. Four-μm sections of formalin-fixed, paraffin-embedded rodent mammary glands, lungs, and human breast tissues were pretreated with Dako EDTA antigen retrieval solution (Dako S2367) (LYVE1, CC3, D2-40) or Dako TRS Antigen Retrieval Solution (Dako S1699) (COX-2) at 125°C under pressure for 5 minutes. All tissues were blocked with 3% H_2O_2 (diluted in methanol) for 10 minutes and Dako Protein Block (X0909) for 10 minutes, respectively. Rodent tissue was incubated with LYVE1 antibody (Abcam 33682) at 1:400 dilution, CC3 antibody (Cell Signaling Technology 9661) at 1:100 dilution, or COX-2 (Cayman 160112) at 1:400. After antigen retrieval in pressure, human tissue was incubated with D2-40 antibody (Dako M3619) at a 1:50 dilution. Sections were incubated with primary antibody for 1 hour followed by Dako EnVision$^+$ System HRP rabbit (K4003) or Dako EnVision$^+$ System HRP mouse secondary (K4001) antibodies for 30 minutes. All tissues were incubated with the chromogen 3,3′-diaminobenzidine (Dako K346811) for 10 minutes and then counterstained with hematoxylin for 6 minutes. Stained slides images were acquired using a ScanScope T3 scanner at 0.46 μ per pixel.

Lymphatic vessel density and lymphatic invasion analysis. For lymphatic vessel density, LYVE1$^+$ or D2-40$^+$ vessel count was determined by 2 independent blinded observers using Aperio Imaging software, with counts normalized to area. Interoperator counts were within the limits of agreement by Bland-Altman plot. For normal adjacent human breast tissues, histologically normal tissue >1 mm from any tumor tissue present was assessed. Peritumor area was 1 mm for human studies and 1–3 mm for mouse studies. For lymphatic invasion analysis, LYVE1$^+$ or D2-40$^+$ vessels were evaluated for presence of tumor cell nuclei by a breast pathologist blinded to study group.

Analysis of lymph node and lung metastasis. For the xenograft model, micrometastases data were obtained by staining lung tissue sections for GFP and human cytokeratin 5, which MCF10DCIS cells express. Only cells that were dual positive for GFP and cytokeratin 5 were considered metastatic breast tumor cells. For the 66cl4 model, axillary lymph node and lung metastasis were determined primarily using clonogenic assays described previously (31) and, for the lung, metastasis was confirmed by histologic analyses.

In vitro lymphangiogenesis assays. For migration assays, HDLECs were placed atop 8-micron transwell inserts (BD) according to published methods (1), and tumor cells or tumor cell–conditioned media was placed in bottom well as the chemoattractant source. The number of migrated HDLECs was determined by fixing, staining, and counting cells on the filter bottom (1). For tube formation assays, 30,000 HDLECs were seeded on 4 mg/ml Matrigel pads on glass coverslips and incubated with 50% conditioned tumor cell media/50% endothelial cell media for 24 hours. Surface area was calculated using ImageJ to determine surface area of HDLEC structures. Branch points were counted by 2 independent blinded observers. In vitro experiments were replicated 3 times with pooled data shown.

Immunofluorescence. 0.5% Triton X-100 was used for permeabilization, followed by 1.1 M glycine quench, and then cells were blocked with 20 mg/ml BSA. Cells from in vitro tube formation assays were incubated with VE-cadherin primary antibody at 1:200 (Abcam ab33168), followed by Alexa Fluor 594–conjugated goat anti-rabbit secondary antibody. Slides were mounted using VECTASHIELD Mounting Medium with DAPI (Vector Labs). Images were captured using a Zeiss Axioskop microscope equipped with an HBO 100 lamp and a digital camera (SPOT RTke, SPOT Diagnostics).

Protein expression analyses. For VE-cadherin, EP2, and CC3, protein was isolated from HDLECs in the tube formation assays. Cell pellets were lysed (10 mM Tris, pH 7.4, 150 mM NaCl, 0.1% SDS, 1% sodium deoxycholate, 1% Triton X-100, 200 μg/ml PMSF, 1x PI cocktail; Sigma-Aldrich), and equal amounts of protein (between 20 to 100 μg) were electrophoresed on 8% (VE-cadherin) or 10% polyacrylamide gels (200 V for 1 hour at room temperature) and then transferred to nitrocellulose membrane (Amersham Biosciences) at 100 V for 1 hour at room temperature. Membranes were blocked (5% milk, 30 minutes at room temperature) and incubated with the following primary antibodies: VE-cadherin (Abcam 33168) at 1 μg/ml; CC3 (Cell Signal 9664) at 1:500; D2-40 (Dako M3619) at 1:1,000; and GAPDH (Sigma-Aldrich G9545) at 1:1,000, diluted in wash buffer (10 mM Tris-HCl, pH 8.0, 150 mM NaCl, 0.1% Tween-20) overnight (4°C). Three 10-minute washes preceded and followed incubation with secondary anti-rabbit and anti-mouse HRP-conjugated antibodies for 1 hour at room temperature. Pierce ECL Western Blotting Substrate was used to detect chemiluminescence. ImageJ was used for densitometry, with normalization to D2-40 for HDLECs and GAPDH for tumor cells. The Prostaglandin E2 E1A ELISA Kit (Cayman) was used to measure PGE_2 metabolites in conditioned media and tumor cell lysates according to the manufacturer's protocol.

RNA analyses. RNA was isolated from 50 mg whole rat mammary gland tissue using Trizol reagent (Invitrogen). Concentration and purity were determined by 260 nm, 230 nm, and 280 nm fluorescence. cDNA was synthesized from 1,000 ng RNA using the Bio-Rad cDNA Synthesis Kit, and cDNA was amplified using primers for reference gene β-actin (*Actb*) (forward: TTGCTGACAGGATGCAGAAGGAGA, reverse: ACTCCTGCTTGCTGATCCACATCT), VEGFC (forward: CCACGTGAGGTGTGTATAGATG, reverse: CCACGTGAGGTGGTATAGATG), VEGFD (forward: CCCTAGAGAGACATGCGTAGA, reverse: CTCCACACCGGAAGACATTTA), VEGFR2 (forward: GACGACCCATTGAGTCCAATT, reverse: GTGAGGATGACCGTGTAGTTT), VEGFR3 (forward: ACATGCTCTGGTGCTCAAA, reverse: CACCAGCTCCAGACTGATATT), and LYVE1 (forward: GCCTTGTTGGCAGAGACTATA, reverse: GAACATCGGCAACAATGAAGA). qPCR was performed using Bio-Rad SYBR Green Supermix. The conditions were as follows: 95°C for 3 minutes,

then 40 cycles of 95°C for 15 seconds, 60°C for 30 seconds, and 72°C for 30 seconds. mRNA quantification was normalized using the geometric average of the reference gene, *Actb*.

Aperio software analysis. COX-2 expression was quantitated as described previously (1). Lymphatic vessel density was also assessed as described above.

Statistics. Unpaired *t* test, χ^2 test, and Pearson correlations were performed in GraphPad Prism, assuming independent samples and normal distributions. Only *P* values of less than 0.05 were considered significant.

Acknowledgments

We acknowledge K. Polyak and A. Marusyk (Harvard Medical School) for providing MCF10DCIS parental cells and derivatives, M. Reyland (University of Colorado) for C57/BL6 mouse tissues, H. Ford and C. Wang (University of Colorado) for 66cl4-Luc cells, D. Gao (University of Colorado) for statistical analyses, C. Ambrosone (Roswell Park Cancer Institute) and L. Hines (University of Colorado, Colorado Springs) for human tissues, and K. Bell and S. Black for histology and technical assistance. We also want to thank A. Nelson and K. Schwertfeger (University of Minnesota) and S. Haslam (Michigan State University) for critical review of the manuscript. In addition, we gratefully acknowledge the patients for their contribution to this research. This work was supported by the Department of Defense (BC101904), NIH/National Cancer Institute (1R01CA169175), and Avon Family Foundation and Grohne Family Foundation grants to P. Schedin and V.F. Borges; a Breast Cancer Research Foundation–American Association for Cancer Research grant (BCRF-AACR 09-60-26) to V.F. Borges; Colorado CTSI (grant no. KL2 TR001080), Cancer League of Colorado, Komen Foundation (KG111362), and American Cancer Society New England Division Postdoctoral Fellowship Spin Odyssey (116056-PF-08-257-01-CSM) to T.R. Lyons. The authors appreciate the contribution of the Tissue Biobanking and Processing Shared Resource of Colorado's NIH/National Cancer Institute Cancer Center Support grant P30CA046934 and acknowledge the Colorado CTSI (NIH/National Center for Research Resources grant no. UL1 RR025780) for the RedCap resource.

Address correspondence to: Traci R. Lyons or Pepper Schedin, University of Colorado Anschutz Medical Campus, MS8117, 12801 East 17th Ave., Aurora, Colorado 80045, USA. Phone: 303.724.3885; E-mail: Traci.Lyons@ucdenver.edu (T.R. Lyons). Phone: 303.724.3873; E-mail: Pepper.Schedin@ucdenver.edu (P. Schedin).

1. Lyons TR, et al. Postpartum mammary gland involution drives progression of ductal carcinoma in situ through collagen and COX-2. *Nat Med*. 2011;17(9):1109–1115.
2. Lyons TR, Schedin PJ, Borges VF. Pregnancy and breast cancer: when they collide. *J Mammary Gland Biol Neoplasia*. 2009;14(2):87–98.
3. McDaniel SM, et al. Remodeling of the mammary microenvironment after lactation promotes breast tumor cell metastasis. *Am J Pathol*. 2006;168(2):608–620.
4. O'Brien J, et al. Alternatively activated macrophages and collagen remodeling characterize the postpartum involuting mammary gland across species. *Am J Pathol*. 2010;176(3):1241–1255.
5. Jindal S, et al. Postpartum breast involution reveals regression of secretory lobules mediated by tissue-remodeling. *Breast Cancer Res*. 2014;16(2):R31.
6. Schedin P. Pregnancy-associated breast cancer and metastasis. *Nat Rev Cancer*. 2006;6(4):281–291.
7. Gupta PB, et al. Systemic stromal effects of estrogen promote the growth of estrogen receptor-negative cancers. *Cancer Res*. 2007;67(5):2062–2071.
8. Stensheim H, Moller B, van Dijk T, Fossa SD. Cause-specific survival for women diagnosed with cancer during pregnancy or lactation: a registry-based cohort study. *J Clin Oncol*. 2009;27(1):45–51.
9. Johansson AL, Andersson TM, Hsieh CC, Cnattingius S, Lambe M. Increased mortality in women with breast cancer detected during pregnancy and different periods postpartum. *Cancer Epidemiol Biomarkers Prev*. 2011;20(9):1865–1872.
10. Callihan EB, et al. Postpartum diagnosis demonstrates a high risk for metastasis and merits an expanded definition of pregnancy-associated breast cancer. *Breast Cancer Res Treat*. 2013;138(2):549–559.
11. Bono P, Wasenius VM, Heikkila P, Lundin J, Jackson DG, Joensuu H. High LYVE-1-positive lymphatic vessel numbers are associated with poor outcome in breast cancer. *Clin Cancer Res*. 2004;10(21):7144–7149.
12. Van den Eynden GG, et al. Distinguishing blood and lymph vessel invasion in breast cancer: a prospective immunohistochemical study. *Br J Cancer*. 2006;94(11):1643–1649.
13. Arnaout-Alkarain A, Kahn HJ, Narod SA, Sun PA, Marks AN. Significance of lymph vessel invasion identified by the endothelial lymphatic marker D2-40 in node negative breast cancer. *Mod Pathol*. 2007;20(2):183–191.
14. Schoppmann SF, Horvat R, Birner P. Lymphatic vessels and lymphangiogenesis in female cancer: mechanisms, clinical impact and possible implications for anti-lymphangiogenic therapies (Review). *Oncol Rep*. 2002;9(3):455–460.
15. Skobe M, et al. Induction of tumor lymphangiogenesis by VEGF-C promotes breast cancer metastasis. *Nat Med*. 2001;7(2):192–198.
16. Ran S, Volk L, Hall K, Flister MJ. Lymphangiogenesis and lymphatic metastasis in breast cancer. *Pathophysiology*. 2010;17(4):229–251.
17. Gogineni A, et al. Inhibition of VEGF-C modulates distal lymphatic remodeling and secondary metastasis. *PLoS One*. 2013;8(7):e68755.
18. Karnezis T, et al. VEGF-D promotes tumor metastasis by regulating prostaglandins produced by the collecting lymphatic endothelium. *Cancer Cell*. 2012;21(2):181–195.
19. Achen MG, Stacker SA. Molecular control of lymphatic metastasis. *Ann N Y Acad Sci*. 2008;1131:225–234.
20. Stacker SA, et al. VEGF-D promotes the metastatic spread of tumor cells via the lymphatics. *Nat Med*. 2001;7(2):186–191.
21. Mandriota SJ, et al. Vascular endothelial growth factor-C-mediated lymphangiogenesis promotes tumour metastasis. *EMBO J*. 2001;20(4):672–682.
22. Mattila MM, Ruohola JK, Karpanen T, Jackson DG, Alitalo K, Harkonen PL. VEGF-C induced lymphangiogenesis is associated with lymph node metastasis in orthotopic MCF-7 tumors. *Int J Cancer*. 2002;98(6):946–951.
23. Karpanen T, et al. Vascular endothelial growth factor C promotes tumor lymphangiogenesis and intralymphatic tumor growth. *Cancer Res*. 2001;61(5):1786–1790.
24. Hoshida T, et al. Imaging steps of lymphatic metastasis reveals that vascular endothelial growth factor-C increases metastasis by increasing delivery of cancer cells to lymph nodes: therapeutic implications. *Cancer Res*. 2006;66(16):8065–8075.
25. Isaka N, Padera TP, Hagendoorn J, Fukumura D, Jain RK. Peritumor lymphatics induced by vascular endothelial growth factor-C exhibit abnormal function. *Cancer Res*. 2004;64(13):4400–4404.
26. Betterman KL, et al. Remodeling of the lymphatic vasculature during mouse mammary gland morphogenesis is mediated via epithelial-derived lymphangiogenic stimuli. *Am J Pathol*. 2012;181(6):2225–2238.
27. Flister MJ, Volk LD, Ran S. Characterization of Prox1 and VEGFR-3 expression and lymphatic phenotype in normal organs of mice lacking p50 subunit of NF-κB. *Microcirculation*. 2011;18(2):85–101.
28. Pepper MS, et al. Regulation of VEGF and VEGF receptor expression in the rodent mammary gland during pregnancy, lactation, and involution. *Dev Dyn*. 2000;218(3):507–524.
29. Evangelou E, Kyzas PA, Trikalinos TA. Comparison of the diagnostic accuracy of lymphatic endothelium markers: Bayesian approach. *Mod Pathol*. 2005;18(11):1490–1497.
30. Karpanen T, Alitalo K. Molecular biology and pathology of lymphangiogenesis. *Annu Rev Pathol*. 2008;3:367–397.
31. Aslakson CJ, Rak JW, Miller BE, Miller FR.

Differential influence of organ site on three subpopulations of a single mouse mammary tumor at two distinct steps in metastasis. *Int J Cancer*. 1991;47(3):466–472.
32. Karkkainen MJ, et al. Vascular endothelial growth factor C is required for sprouting of the first lymphatic vessels from embryonic veins. *Nat Immunol*. 2004;5(1):74–80.
33. Katori M, Majima M. Cyclooxygenase-2: its rich diversity of roles and possible application of its selective inhibitors. *Inflamm Res*. 2000;49(8):367–392.
34. Smith WL, Dewitt DL. Prostaglandin endoperoxide H synthases-1 and -2. *Adv Immunol*. 1996;62:167–215.
35. Katoh H, et al. COX-2 and prostaglandin EP3/EP4 signaling regulate the tumor stromal proangiogenic microenvironment via CXCL12-CXCR4 chemokine systems. *Am J Pathol*. 2010;176(3):1469–1483.
36. Shi S, Klotz U. Clinical use and pharmacological properties of selective COX-2 inhibitors. *Eur J Clin Pharmacol*. 2008;64(3):233–252.
37. Ramirez RA, Lee A, Schedin P, Russell JS, Masso-Welch PA. Alterations in mast cell frequency and relationship to angiogenesis in the rat mammary gland during windows of physiologic tissue remodeling. *Dev Dyn*. 2012;241(5):890–900.
38. Matsumoto M, Nishinakagawa H, Kurohmaru M, Hayashi Y, Otsuka J. Pregnancy and lactation affect the microvasculature of the mammary gland in mice. *J Vet Med Sci*. 1992;54(5):937–943.
39. Djonov V, Andres AC, Ziemiecki A. Vascular remodelling during the normal and malignant life cycle of the mammary gland. *Microsc Res Tech*. 2001;52(2):182–189.
40. Fornetti J, Jindal S, Middleton KA, Borges VF, Schedin P. Physiological COX-2 expression in breast epithelium associates with COX-2 levels in ductal carcinoma in situ and invasive breast cancer in young women. *Am J Pathol*. 2014;184(4):1219–1229.
41. Bhattacharjee RN, Timoshenko AV, Cai J, Lala PK. Relationship between cyclooxygenase-2 and human epidermal growth factor receptor 2 in vascular endothelial growth factor C up-regulation and lymphangiogenesis in human breast cancer. *Cancer Sci*. 2010;101(9):2026–2032.
42. Kerjaschki D. The crucial role of macrophages in lymphangiogenesis. *J Clin Invest*. 2005;115(9):2316–2319.
43. Schoppmann SF, et al. Tumor-associated macrophages express lymphatic endothelial growth factors and are related to peritumoral lymphangiogenesis. *Am J Pathol*. 2002;161(3):947–956.
44. Hall KL, Volk-Draper LD, Flister MJ, Ran S. New model of macrophage acquisition of the lymphatic endothelial phenotype. *PLoS One*. 2012;7(3):e31794.
45. O'Brien J, Martinson H, Durand-Rougely C, Schedin P. Macrophages are crucial for epithelial cell death and adipocyte repopulation during mammary gland involution. *Development*. 2012;139(2):269–275.
46. Rothwell PM, Wilson M, Price JF, Belch JF, Meade TW, Mehta Z. Effect of daily aspirin on risk of cancer metastasis: a study of incident cancers during randomised controlled trials. *Lancet*. 2012;379(9826):1591–1601.
47. He Y, Karpanen T, Alitalo K. Role of lymphangiogenic factors in tumor metastasis. *Biochim Biophys Acta*. 2004;1654(1):3–12.
48. Karpanen T, et al. Lymphangiogenic growth factor responsiveness is modulated by postnatal lymphatic vessel maturation. *Am J Pathol*. 2006;169(2):708–718.
49. Dunworth WP, Fritz-Six KL, Caron KM. Adrenomedullin stabilizes the lymphatic endothelial barrier in vitro and in vivo. *Peptides*. 2008;29(12):2243–2249.
50. Fritz-Six KL, Dunworth WP, Li M, Caron KM. Adrenomedullin signaling is necessary for murine lymphatic vascular development. *J Clin Invest*. 2008;118(1):40–50.
51. He Y, et al. Suppression of tumor lymphangiogenesis and lymph node metastasis by blocking vascular endothelial growth factor receptor 3 signaling. *J Natl Cancer Inst*. 2002;94(11):819–825.
52. Callihan EB, et al. Postpartum diagnosis demonstrates a high risk for metastasis merits an expanded definition of pregnancy-associated breast cancer. *Breast Cancer Res Treat*. 2013;138(2):549–559.
53. Pilewskie M, et al. Association between recency of last pregnancy and biologic subtype of breast cancer. *Ann Surg Oncol*. 2012;19(4):1167–1173.
54. Wang CA, et al. SIX1 induces lymphangiogenesis and metastasis via upregulation of VEGF-C in mouse models of breast cancer. *J Clin Invest*. 2012;122(5):1895–1906.
55. Hu M, Peluffo G, Chen H, Gelman R, Schnitt S, Polyak K. Role of COX-2 in epithelial-stromal cell interactions and progression of ductal carcinoma in situ of the breast. *Proc Natl Acad Sci U S A*. 2009;106(9):3372–3377.